RSC Advances

PAPER

View Article Online
View Journal | View Issue

Cite this: *RSC Adv.*, 2021, **11**, 16675

Enhanced thermoelectric performance of graphene based nanocomposite coated self-powered wearable e-textiles for energy harvesting from human body heat†

Nazakat Ali Khoso,[a] Xie Jiao,[a] Xu GuangYu,[a] Sun Tian[c] and JiaJun Wang*[b]

The demand for highly flexible and self-powered wearable textile devices has increased in recent years. Graphene coated textile-based wearable devices have been used for energy harvesting and storage due to their outstanding mechanical, electrical and electronic properties. However, the use of metal based nanocomposites is limited in textiles, due to their poor bending, fixation, and binding on textiles. We present here reduced graphene oxide (rGO) as an n-type and conductive polymer poly(3,4-ethylenedioxythiophene) polystyrene sulfonate (PEDOT:PSS) as a p-type material for a wearable thermoelectric nanogenerator (TEG) using a (pad–dry–cure) technique. We developed a reduced graphene oxide (rGO) coated textile-based wearable TEG for energy harvesting from low-grade human body heat. The conductive polymer (PEDOT:PSS) and (rGO) nanocomposite were coated using a layer by layer approach. The resultant fabric showed higher weight pickup of 60–80%. The developed textile based TEG device showed an enhanced Seebeck coefficient of (25–150 μV K^{-1}), and a power factor of (2.5–60 μW m^{-1} K^{-1}). The developed TE device showed a higher potential to convert the low-grade body heat into electrical energy, between the human body temperature of (36.5 °C) and an external environment of (20.0 ± 5 °C) with a temperature difference of (2.5–16.5 °C). The wearable textile-based TEG is capable of producing an open circuit output voltage of 12.5–119.5 mV at an ambient fixed temperature of (20 °C). The rGO coated textile fabric also showed reduced electrical sheet resistance by increasing the number of dyeing cycles (10) and increased with the number of (20) washing cycles. The developed reduced graphene oxide (rGO) coated electrodes showed a sheet resistance of 185–45 kΩ and (15 kΩ) for PEDOT:PSS–rGO nanocomposites respectively. Furthermore, the mechanical performance of the as coated textile fabric was enhanced from (20–80 mPa) with increasing number of padding cycles. The thermoelectric performance was significantly improved, without influencing the breath-ability and comfort properties of the resultant fabric. This study presents a promising approach for the fabrication of PEDOT:PSS/rGO nano-hybrids for textile-based wearable thermoelectric generators (TEGs) for energy harvesting from low-grade body heat.

Received 23rd December 2020
Accepted 22nd April 2021

DOI: 10.1039/d0ra10783b

rsc.li/rsc-advances

1. Introduction

The development of graphene coated textile based wearable energy harvesting and storage devices is highly anticipated with low grade body heat as a green and sustainable technique. The demand for such highly flexible and breathable wearable e-textiles is increasing due to their use in energy storage, conversion, and harvesting devices.[1] The human body is a highly stable form of energy source for energy harvesting, which can be used for wearable health monitoring devices.[2] We used a new approach in mass scale fabrication of graphene based wearable and washable e-textiles for future research in which the thermoelectric fabric is integrated as an energy harvesting device from human body heat.[3] The developed textile may replace metal based wearable textiles with advanced electronic and electrical properties and may provide a new window for the development of novel technologies which can be used for self-powered health monitoring devices, disease diagnostics, and prevention.[4] In brief, the TE material should possess an improved Seebeck coefficient S, as well as higher electrical conductivity σ. Whereas, the low thermal conductivity κ[5] is good for TE materials to operate a steady level of heat flow into electrical energy; because a high-performance thermoelectric material may hold a large thermal gradient as a temperature difference required to keep in the output electric potential

[a]*College of Materials and Textiles, Zhejiang Sci-Tech University, Hangzhou, Zhejiang, PR China*

[b]*School of Art and Design, Zhejiang Sci-Tech University, Hangzhou, Zhejiang, PR China. E-mail: Wangjjhz@163.com*

[c]*Shanghai Institute of Ceramics, Chinese Academy Sciences (CAS), Shanghai, PR China*

† Electronic supplementary information (ESI) available: Thermoelectrics, body heat. See DOI: 10.1039/d0ra10783b

difference.[6] The Seebeck voltage, is attained even though with a small temperature difference which is near to room temperature, even human body temperature. The TE parameters, σ and S are reciprocal to an electrical conductivity,[7] whereas the σ and κ_e are directly related with each other. In connection of relationship to these invariable factors to enhance the dimension less figure of merit ZT, which is highly challenging to be improved.[8] On the other hand, the thermoelectric power factor is addressed as $PF = S^2\sigma$, in which assess the concomitant effect of σ and S on TE performance.[9] Compared to inorganic counterparts, organic TE devices emerged as the potential candidates work at room-temperature and flexible (even wearable) TE power generation. During last few decades, extensive studies have been performed on the p- and n-type materials and devices to build up the inter-relationship among the TE parameters (*i.e.*, electrical conductivity, Seebeck coefficient, thermal conductivity and power factors), demonstrating a great potential of organic TEs.[10] Hence, the use of organic materials such as carbon and its derivatives are highly anticipated for multifunctional finishing of textiles. The demand of carbon-based allotropes such as fullerene, carbon black (CB), carbon nanotubes (CNT), graphite oxide (GrO), graphene oxide (GO), reduced graphene oxide (rGO) and graphene is increasing in recent years for wearable flexible, bendable, breathable and washable electronic devices.[11,12] The use of conductive polymers with graphene and its derivatives is also highly attractive and considered as potential materials as compared to traditional metal-coated e-textiles. Therefore, the use of an organic conducting polymers such as: poly(3,4-ethylenedioxythiophene) (PEDOT) EDOT:$FeCl_3$,[13] EDOT:FeToS,[14] polyaniline (PANI),[15] polypyrrole (PPy),[16] and poly(3-hexylthiophene) (P3HT)[17] are considered as promising materials for organic TE devices. The improved TE performance in these conducting polymers based of thiophene polymer poly(3,4-ethylenedioxythiophene) (PEDOT) has been reported. The intrinsic conductive polymer showed an enhanced TE performance with PF of 469 $\mu W\ m^{-1}\ K^{-2}$ and dimension less figure of merit ZT value of 0.42 at room temperature when doped with poly(styrenesulfonic) (PSS) in conductive polymer.[18] Among all these conducting polymers, polyaniline (PANI) is also well known and most widely used polymer which have an electrical conductivity σ of 105 $S\ m^{-1}$, as comparable to the state-of-the-art for all inorganic TE materials.[19] The polymer is considered as highly environmentally stable and dipped with graphene, graphite, carbon black and CNTs have easy and high dissolution in PANI, which make them more easier to be dispersed in PANI.[20] As well as reported in study, that these polymer develops strong bonding and exists a strong π–π interaction between the polymer PANI intermolecular and intramolecular with carbon based derivatives.[21] The addition of these filler which would allows stable and enhanced growth of molecular chains for graphene in an ordered polymer matrix with PANI polymer chains with surface of carbon materials.[22] The another conductive polymer including polythiophene (PTh) showed a low Seebeck coefficient (S) and less electrical conductivity σ. The TE performance is significantly influenced by the size, shape, crystal growth, and orientation of the side chains with main chain structure in the nanocomposites.[23] The overall TE performance obtained with this polymer is nearly exhibiting a high S of ~130 and 76 $\mu V\ K^{-1}$, $\sigma \sim 47$ and 73 $S\ cm^{-1}$, under lower thermal conductivity κ of 0.17 and 0.15 $W\ m^{-1}\ K^{-1}$, respectively at room temperature.[24] The thermoelectric properties in fine-tuned by doping or dedoping of the polymeric materials, using various organic and inorganic filler, in which the Seebeck coefficient was significantly improved whereas, on the other hand the electrical conductivity of the developed nanocomposites was decreased, similar to attributes of inorganic materials.[24] However, as compared to inorganic thermoelectric materials, the intrinsic conductive polymers such as PEDOT:Tos films showed relatively less thermal conductivity of 0.2–0.25 $W\ m^{-1}\ K^{-1}$. On the otherhand, the power factor was also raised from 38 to 324 $\mu W\ m^{-1}\ K^{-2}$, with a figure of merit (ZT) value of 0.25 at room temperature.[25] The carrier concentration improved the filtering effect and showed a favorable TE results which contributed as higher Seebeck coefficient of (163 $\mu V\ K^{-1}$) and power factor of (70.9 $\mu W\ m^{-1}\ K^{-2}$) during doping in the conductive polymers *i.e.* poly(3,4-ethylenedioxythiophene):poly(styrenesulfonate).[26] Familiarly, the development of inorganic doped in conductive polymer (PEDOT:PSS)/Te) introduced the Te nanorods in the nanocomposites with improved interfaces.[27] Similarly, the nanocomposites of PANi/graphene–PEDOT:PSS/PANi/DWCNT–PEDOT:PSS has been fabricated using layer-by-layer (LBL deposition) on different textile substrates.[28] The conductive polymer PEDOT:PSS was used developed nanocomposites using some surfactants *i.e.* (SDS) (SDBS) to disperse and stabilize the graphene and CNTs dispersion. The resultant nano-composite showed an electrical conductivity σ of 190 $S\ cm^{-1}$, Seebeck coefficient (S) of 120 $\mu V\ K^{-1}$ and power factor PF of 2710 $\mu W\ m^{-1}\ K^{-2}$. Their results shows that, the best inorganic TE material Bi_2Te_3 exhibits improved TE performance at room temperature.[29] The another work discuses, that the higher increase in carrier mobility efficiently increased the electrical conductivity σ, and reduced the TE performance in terms of Seebeck coefficient and power factor by the reduction of the carrier concentration with a decreased Seebeck coefficient, as well as favorable raising in the PF of 220 $\mu W\ m^{-1}\ K^{-2}$, which is twice higher magnitude than the PANI–CSA (~1.8 $\mu W\ m^{-1}\ K^{-2}$ these results are reported in previous studies performed on PANI nanocomposites.[30] The another study made on the optimization of TE performance in terms of Seebeck coefficient, PF for the PANI–CNT based nanocomposites. The results demonstrated that the TE performance was improved as compared to the pristine CNT and graphene film. Another study, researchers developed highly conductive polymer polyaniline (PANI)/with (SWCNTs) nanocomposites using *in situ* polymerization and template free approach for TE devices.[31] It was found that the solution processing and strong π–π interactions between the PANI and SWCNTs induced the PANI molecules to form a highly ordered structure. This improved degree of order of the PANI molecular arrangement increased the charge carrier mobility and thereby enhanced the electrical transport properties of PANI. The PANI/SWCNT (65 wt%) composite films (10 μm) exhibited an electrical conductivity, Seebeck coefficient, and power factor of $1.44 \times 10^3\ S\ cm^{-1}$, 39 $\mu V\ K^{-1}$ and 217 $\mu W\ m^{-1}\ K^{-2}$ respectively at room temperature.[32] This PF was more than 20 times the PF of pure PANI film. The

improvement in TE properties is attributed to the highly ordered structure of PANI chains along the SWCNT *via* strong π–π interaction,[33] which turned into increased the carrier mobility. The quantum Hall effect measurement showed that the charge carrier mobility improves with increasing of concentration, while the charge carrier mobility increased three times with the increasing the content percent of CNT in the polymer nanocomposite. Furthermore, the thermal conductivity out of plane was very low of 0.2–0.5 W m^{-1} K^{-1} at room temperature.[34] Such polymer based composites are generally fabricated using *in situ*, chemical oxidation, vapor phase polymerization, and chemical exfoliation,[35–37] whereas the filler are widely mixed with different organic solvents, reducing agents, dispersing agents and stabilizers.[38] The features of the intrinsic conductive polymers are not only limited to their potential electrical and thermal properties but due to their light weight, flexibility and higher stability against water, and air makes them highly suitable for super capacitors, batteries, solar cells, and other energy storage and harvesting devices.[39] Furthermore, chemical functionalization and *in situ* solution processed polymer composite are commonly used including screen printing, ink jet printing dispenser printing; spray printing, and spin coating,[40,41] as an efficient, cost-effective method to fabricate TE devices on mass scale. The use of inorganic metals such as silver, copper, and gold based wearable devices become limited due to their higher rigidity, stiffness, and decomposition when exposed to water and air.[42] These metal-based electronic devices need intense care during fabrication and use as heavy batteries embedded in clothes are less flexible, highly stiff, non-biodegradable and toxic to human skin as well environment.[43] The use of graphene with these conductive polymer coated e-textiles has been used for various applications including super capacitors, batteries, pressure sensors, thermoelectric, triboelectric, piezoelectric, and nano-generators.[44–46] However, the production of graphene-based highly flexible, breathable and stretchable thermoelectric devices is challenging and need further improvements for mass production. The synthesis and fabrication of such a highly conducive, breathable, and washable textiles is complicated and limited due to their production on a commercial scale. The widely used fabrication processes are complicated, time-consuming and expensive. Some of these techniques include chemical, and thermal reduction of reduced graphene oxide (rGO) coated fabrics has been reported in the previous studies.[47] Thermal reduction is achieved at higher temperature range of 150–200 °C which is more costly and time-consuming. Whereas, synthetic fibers such as polyester, acrylic, Lycra, and spandex are susceptible to excessive heat, which results in deformation of the polymer chains at higher temperature range above glass transition temperature (T_g) 160–200 °C.[48] Fabrication of graphene and other carbon-based materials require chemical and thermal treatment with strong reducing agents such as, hydrazine hydrate (HH), hydro iodic (HI), sodium borohydrate ($NaBH_4$).[49] The use of these reducing agents is insecure and limited, as wearable textile directly contacts with human skin can induce skin-irritation, and other allergic reactions.[50] The natural fibers such as cotton, jute, flex and hemp fibers lose strength due to the polymer degradation as their basic monomer is cellulose. The use of highly efficient and green reducing agents is needed for the production of rGO coated wearable e-textiles.[51] In this context, several studies have been made so far, by using green reducing agents such as, ascorbic acid ($C_6H_8O_6$), thio-urea (CH_4N_2S), and sodium hydrosulphite ($Na_2S_2O_4$).[52–54] Furthermore, different fabrication techniques has been reported so far; in previous studies, including; vacuum filtration, brush painting, spin coating, spray coating, screen printing, stencil printing, dip coating, heat transfer, vapor deposition, chemical vapor deposition (CVD) and wet transfer.[55] Among all, pad–dry–cure method is an efficient process with processing rate of 150 m min^{-1}, suitable for mass production of graphene-coated textiles.[56] Whereas, the graphene is hydrophobic and cannot be dispersed in water and other ionic solvents; therefore the fixation of carbon-based materials on textiles is also limited. As dispersion of graphene and carbon material is only possible with the addition of certain dispersing agents and anionic surfactants including, sodium dodecyl sulphonate (SDS), sodium dodecyl benzene sulphonate (SDBS), ammonium persulphate (APS) and cetyltrimethylammonium bromide; hexadecyltrimethylammonium bromide (CTAB).[57–60] Application and fixation of graphene is accomplished either by covalent or non-covalent chemical functionalization using ionic liquids including dimethyl sulphoxide (DMSO), and dimethyl formamide (DMF).[61–63] Several binders and thickeners such as polyurethane (PU), polyvinyl alcohol (PVA), polyvinylidene fluoride (PVDF), polystyrene (PS), polystyrene sulphone (PSS), carboxy methyl cellulose (CMC), sodium alginate, water-borne polyurethane (WPU), and polyvinylidenes (PVP) have also been used.[64–69] The use of such binders, thickeners and dispersing agents may influence the physical properties such as luster, feel, touch and end use properties for example; electrical, thermal, mechanical and comfort characteristics by altering transport of water vapors and air permeability of wearable e-textiles.[70–72]

In this study, we used commercial-scale technique for the development of graphene coated cotton textile fabric for wearable thermoelectric nanogenerator for energy harvesting from low grade body heat. The as dyed fabric was converted into rGO using green reducing agent (L-ascorbic acid) and lower scale thermal reduction at (90 °C) which is more convenient and efficient as compared other high temperature thermal reduction techniques. Herein, this study we applied GO as a dye in a water based dispersed solution of PEDOT:PSS without using any binder and dispersing agent. The application process uses already commercialized pad–dry–cure simple dyeing technique approach. This study demonstrates; that pad–dry–cure method is an alternative approach for the development of conductive textiles, which assists in better fixation and adhesion of graphene on textiles without using any binder or thickener.

2. Experimental

2.1 Materials and methods

Carbon material graphite of (Grade 3061) was obtained from Asbury Graphite Mills, USA, poly(sodium 4-styrene sulfonate) (PEDOT:PSS) 1.2% H_2O of highly conductive grade was purchased from Sigma Aldrich Shanghai. L-Ascorbic acid (vitamin C) obtained from Sigma Aldrich, Shanghai, ammonia (NH_3), potassium permanganate ($KMnO_4$), sulfuric acid (H_2SO_4, ~99%), hydrogen peroxide (H_2O_2, ~30%), were purchased from

Sigma-Aldrich and XFS-Nano Chemical suppliers of Jiangsu and Shanghai. 100% cotton fabric with weave structure of 3/1 twill was provided by Hangzhou Textile Dyeing and Finishing Co. Ltd. Deionized (DI) water was used throughout the study.

2.1.1 Synthesis of GO and reduction (rGO). Graphene oxide (GO) was synthesized using modified Hummer's methods as reported in previous studies.[73] Briefly, the pure graphite was oxidized in three steps; strong oxidation, moderate and high oxidation using sulphuric acid (H_2SO_4), $KMNO_4$ and hydrogen peroxide (H_2O_2) respectively. Initially, pristine graphite by weight (2.5 g) was carried for synthesis. Subsequently, $KMnO_4$ solution was developed using (50 mg of $KMnO_4$ by dissolving in 10.0 ml DI water) added into the above solution. The above mixture was stirred using magnetic stirrer over 250 rpm until the homogeneous mixture was formed. During the reaction, the colour of the solution was changed from black to dark brown and the light reddish. Followed by, 10–30 ml of strong oxidizing agent hydrogen peroxide (H_2O_2) was added drop wise after raising temperature to 80–90 °C. The final product (GO) was obtained as yellow coloration of solution and separated by centrifugation, washed several times with DI water and ethanol and finally dried in a vacuum oven for 24 h at 60 °C. After that, the as obtained graphitic oxide GO coated fabric was reduced into (rGO) using green reducing agent L-ascorbic acid with different weight percent (2.5, 5.0 and 10.0%) using microwave assisted chemical and thermal reduction at 90 °C for 2–3 h.[74]

2.1.2 Fabrication of thermoelectric nanogenerator (TENG). The GO solution with different concentrations (2.5, 5.0, 10.0 and 20.0 mg/250 ml) was dispersed in deionized water to prepare the dyeing solution. The aqueous solution of GO with a liquor ratio of (1 : 20) was directly applied on the cotton fabric using the pad–dry–cure method.[75] The GO coated (multiple dip and nip) cotton fabric was reduced *via* L-ascorbic acid aqueous solution and dried at 90 °C for 1 h in a vacuum dryer.[76] Later on, the resultant rGO coated cotton fabric was coated with PEDOT:PSS using simple drop-casting to develop the thermoelectric (TE) legs. Finally, the prepared fabric samples were analysed for electrical and thermoelectric effect of rGO/PEDOT:PSS as (p-type) and rGO as (n-type) materials.

3. Characterization

Nicolet 5700 the elemental analysis of the graphene oxide, reduced graphene oxide, and PEDOT:PSS–rGO were analyzed using FTIR, Raman, XRD and XPS spectroscopy. A K-alpha mode on XPS (Thermofisher USA), X-ray diffraction (XRD), and (XPS) used to describe the rGO, GO, and PEDOT:PSS–rGO films and nano-composites. The scanning electron microscopy (SEM) analysis of the sample was performed by using a Zeiss ultra-scanning electron microscope (SEM) for the surface of the treated and untreated fabrics. Nicolet 5700 Thermofisher, (USA) was used for FTIR/ATR analysis of the GO, rGO, and PEDOT:PSS–rGO powder of the nano-composites films and coated fabric. A K-alpha mode on XPS (Thermofisher, USA), X-ray diffraction (XRD), and (XPS) used to describe the rGO, GO, and PEDOT:PSS–rGO films and nano-composites. The NEXUS-XPS was recorded using an XPS spectrometer with a monochromatic Al K-α source of 1486.68 eV. The electrical performance of the rGO and PEDOT:PSS decorated cotton fabric was measured by using a four-point probe (SZT-2B) system (Suzhou Genesis Electronics Co. Ltd., China). The average test results with a low sheet resistance of each sample were measured six times and recorded for statistical analysis. The electrical performance of the rGO and PEDOT:PSS decorated cotton fabric was measured by using a four-point probe (SZT-2B) system (Suzhou Genesis Electronics Co. Ltd., China).

3.1 FESEM

The SEM of rGO decorated fabric showed the smooth distribution of rGO films, and developed more significant interaction between PEDOT:PSS–rGO films. The resultant PEDOT:PSS–rGO nanocomposite showed strong interactions with improved π–π bonding between rGO and PSS chains *via* hydrophilic groups on the textile substrate due to the presence of PSS as a binder present in PEDOT:PSS on the surface of cotton fiber as shown in Fig. 2a–c respectively; see Fig. 2 (ESI-S1).† Fabrication of graphene on textiles using the conventional techniques such as dip-coating, spray coating may results uneven distribution of rGO on the surface of fibres. The proposed method shows highly staged graphene layers between yarn and fibres with uniform and smooth coatings, as compared to previous studies.[76] The result shows that, the particle size for the conductive polymer (PEDOT) and PSS as compared to GO, rGO and nanocomposite respectively is shown in Fig. 1 and 2 respectively for FESEM images and EDS elemental analysis showing sufficient coating of carbon element on fabric after reduction. The SEM images were further analysed using the MountainsMap software version 2.0, surface topography and morphological IR colour rendering mode as shown in Fig. 2a′–c′ respectively presented in Fig. 1 and 2 (ESI-S1).† The SEM images demonstrates that, the surface coating of fabric with different

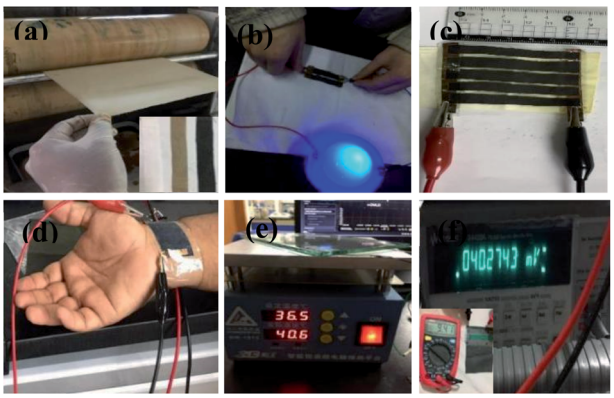

Fig. 1 Fabrication of conductive textiles (a) GO coating on padder machine, fabric GO and rGO coated fabric strips compared to pristine fabric (b) sheet resistance of rGO coated fabric with different cord length (cm) connected with LED light (c) stretching and bending of TE generator connected with 2-probe digital voltmeter for sheet resistance (d) TE nanogenerator attached to human wrist (e) Seebeck measurement setup with controlled thermal gradient (f) output open circuit (mV) obtained from TENG using Keysight digital and analog voltmeter.

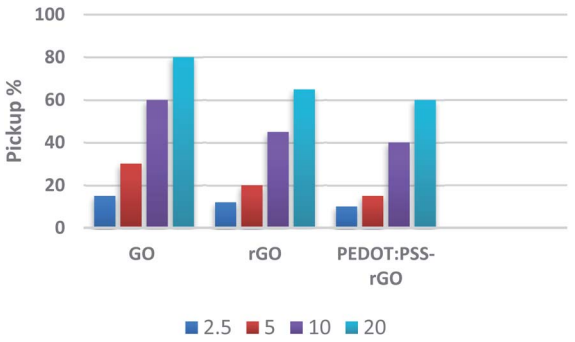

Fig. 2 Effect of rGO content percent 2.5, 5.0, 10.0 and 20.0 on weight pickup percentage of textile substrate coated with GO, rGO and PEDOT:PSS-rGO.

colour codes. The reddish yellow colour shows hot surface as coated with rGO and PEDOT:PSS in green colour as cold hetero junctions on the single fiber surface, whereas the blue colour shows free space among fibers. The IR images well describe the thermal (heat) dispassion of body heat by the graphene layers on the fiber surface.

3.2 X-ray diffraction (XRD)

The XRD results are presented in Fig. S3a† showing GO, rGO, PEDOT:PSS–GO and PEDOT:PSS–rGO nanocomposites respectively. The XRD patterns of GO are located at 10.5° (001) crystal planes with *d*-spacing of (0.83–0.85 nm) as compared to pristine graphite having sharp peak allocated at 26.3–28.5. The peaks become widened and shifted towards 16.5–21.2° (002) with a *d*-spacing of (0.32–0.36 nm); which is near to graphitic *d*-spacing of (d = 0.339) of pure graphite when GO is chemically and thermally reduced into rGO as shown in Fig. S3a and b† respectively; see ESI-S1 Fig. S3a.† The peaks are more widen and shifted from 12.6–16.4° (111) for rGO; occurred due to the thermal annealing and resulted as increase in crystal size and inter layer spacing between graphene sheets after chemical and thermal reduction. The broader peaks of GO located at 16.3° which correspond to the enriched PEDOT ad PSS chains present in the polymer structure. While the sharp peaks located at 25.3° corresponding to the (002) crystallization of graphene sheets re-staging/graphitization of reduction planes of PEDOT crystals heat treatment.[77]

3.3 Raman spectra

Raman spectra reflect the defects and disordered structures of carbon-based materials. The spectral analysis of (GO) and (rGO) showed D and G bands (1350 cm^{-1}, 1355 cm^{-1}, 1345 cm^{-1}) and (1595 cm^{-1}, 1600 cm^{-1}, 1590 cm^{-1}) with the improved intensity ratios (I_D/I_G) from 0.94 for GO to 0.85 for PEDOT:PSS–rGO and 1.06 for pristine rGO which indicates that lower (I_D/I_G) ratio with highly disordered few layered graphene. Whereas the (2G/2D) ratio is totally disappeared, which also indicates, that the textile substrate coated with few layered graphene. The spectral peaks of PEDOT:PSS–rGO over a range of 1356 cm^{-1}, 1435 cm^{-1}, 1431 cm^{-1}, 1425 cm^{-1} and 1585 cm^{-1}, 1583 cm^{-1}, and 1575 cm^{-1} as shown in Fig. S3b.† Whereas, G and D peaks are attributed to the sp^3 to sp^2 hybridization of carbon atoms as shown in see ESI-S1 Fig. S3b.† [78] The small vibration dangling peaks in between D and G which reflects the defects and the disordered structures of graphene films due to the presence of PEDOT and PSS. The broader and widened D and G bands located at 1358 cm^{-1}, (1589 cm^{-1}) demonstrating few layered graphene as compared to graphitic sharp peaks. The developed nanocomposites showed strong interactions of conjugated PEDOT:PSS with reduced graphene oxide sheets, which may attribute to available carboxy (C–C), carbonyl (C=C) and epoxy (O–C–O) functional groups present in reduced graphene oxide after chemical and thermal reduction.[79] Furthermore, the Raman spectra shows small defective peaks in between broader D and G bands of rGO, which may attribute to the availability of PEDOT and PSS. These peaks are allocated to positions 1428 cm^{-1}, 1435 cm^{-1}, 1425 cm^{-1} and 1475 cm^{-1} indicates the π–π conjugation of aromatic rings with higher interfaces of rGO and PEDOT:PSS.[39] It is concluded from the Raman spectra, that rGO have higher interaction with PEDOT, which may attributed to phase separation of PSS and PEDOT resulting improved electrical conductivity with highly ordered PEDOT chains in the nanocomposite.[80]

3.4 XPS analysis

The elemental analysis was performed using X-ray photo spectroscopic using survey peaks and each element analysis of carbon (C 1s) and oxygen (O 1s) elements, after reduction of GO coated cotton fabric into rGO and PEDOT:PSS–rGO nanocomposites. The XPS analysis as shown in ESI-S1 Fig. 4a–d† shows the elemental analysis of carbon (C 1s), oxygen (O 1s), sulphone (S) groups and survey peaks respectively. The XPS analysis also demonstrate that the increasing the number of padding cycles and reducing agents significantly improved (C/O) ratio of the rGO coated cotton fabric. The effect may occur due to the increase of few layered rGO films and chemical reduction of GO into rGO with less oxygen element and enhanced carbon (C) element respectively. The results clearly demonstrate the presence of carbon and oxygen reactive functional groups with different bonds structures; as carbon–carbon (C–C) and (C=C) excited at 284.8 to 284.8, respectively. Whereas, the broader peaks show (C=C) bond structure 284.7 to 284.2, and (C–C) peaks located at 284.2 to 285.7, respectively. Another functional, group epoxy groups (C=O) is available at 287.2 to 286.4, respectively. Whereas, very small peaks available at 289.0, which shows the confirmation of the functional groups (O=C–O) after chemical and thermal reduction of GO into rGO.[81]

Furthermore, carbon to oxygen (C/O) ratio of GO coated cotton is to 3.29, which is increased to 8.0 when GO converted into rGO as shown in Table 1. The XPS analysis shows that content percent of rGO significantly increased the (C/O) ratio, which confirms the adequate loading of rGO on the surface of fibres. The comprehensive scan XPS investigation showed further confirmation of rGO, with the increase of carbon content from 83.3%, 85.7%, and 87.4% for rGO coated cotton as

Table 1 Carbon to oxygen (C/O) ratio of XPS analysis of textiles coated with rGO

Sample	C (%)	O (%)	C/O	Ref.
Untreated	72.9	24.1	3.02	82
GO	73.7	22.4	3.29	83
rGO AA	82.8	14.2	5.83	84
rGO $NaBH_4$	78.5	20.7	3.79	85
rGO HH	83.6	13.3	6.26	86
rGO $Na_2S_2O_4$	85.5	14.0	6.15	87
rGO (AA) 10% coated 1–5 dips	83.3	16.5	4.86	This work
rGO (AA) 10% coated 5–10 dips	85.7	13.4	6.24	This work
rGO (AA) 10% coated (15-dips)	87.4	10.6	8.0	This work

compared to natural cotton and GO ad rGO with 10% of L-ascorbic acid. The research findings of the study also compared with previously reported studies on cotton fabric are shown in Table 1.

4. Measurements

4.1 Weight pick up

The wet pick-up percent of GO was increased significantly from 40% first five padding passes to 80% for several numbers of padding passes shown in Fig. S5a.† The GO showed even better adhesion due to the availability of carboxyl (C=C), carbonyl (C–C), carboxy (C–O) and significantly hydroxyl groups (OH–) present in GO and PEDOT:PSS as reported in previous studies.[88] Whereas, the PEDOT:PSS–rGO showed low pickup percentage as compared to pristine GO. On the other hand, the rGO showed minimum pick up percentage due to low dispersion in water and other solvents. This effect may occur due to the less reactive hydroxyl groups (OH–) functional groups, carboxy, carbonyl and epoxy groups present in GO and rGO respectively. The negatively charged reactive groups (PSS) present in the conductive polymer may also increase the bonding and fixation of graphene on textile substrate. The wet-pick up percentage of graphene on the textile substrate was calculated using the following eqn (1);

$$\text{Pick up\%} = (\text{coated fabric wt} - \text{untreated fabric wt})/\text{untreated fabric dry wt} \times 100 \quad (1)$$

The mean lateral dimension of GO is stable over very few numbers of padding passes, and the size of flakes increased from 25–100 to 100–150 nm as shown in Fig. S5b.† The increase in flake size of GO is due to the reduction into rGO, which may occurred due to the re-connecting of films, which may result an increase in size of the rGO films. Therefore, the (rGO) based dye solution needs to be vigorously stirred and subjected to pre-mixing with ultra-sonication before application on padder for better adhesion to fibers. The Fig. 3 shows that the particle size distribution for the different solution of GO, rGO, and PEDOT:PSS–rGO increased the particle size of GO films from 80, 150–200 and 200–250 nm for rGO and rGO–PEDOT:PSS respectively. The results indicate that the size distribution of the nanoparticles, shifted towards larger particle size for PEDOT:PSS–rGO, which may attribute to the presence of cross-linking polymer (PSS) covering the reduced graphene oxide films.[89]

4.2 Water contact angle (WCA)

The water contact angle test was performed according to ASTM standard D-5725-99 (ref. 90) to analyse the hydrophobic and hydrophilic of the resultant rGO and PEDOT:PSS coated fabric samples. Fig. 4, clearly shows that the fabric becomes highly hydrophobic behaviour due to the rGO. As reduced graphene oxide increased the contact angle which confirms the reduction of GO into rGO as the fabric become hydrophobic. The pure cotton and GO coated cotton fabric showed a lower contact angle of 73°, 115°, and 135°. The water contact angle (WCA) was increased from 48°–95° for rGO-1 to rGO-2, which is further enhanced with increasing the content percent of rGO resulting as super hydrophobic behaviour of the textile substrate with a contact angle of 115°–141° as shown in Fig. 4.

4.3 Tensile strength

The tensile strength of the treated and untreated cotton, GO dyed cotton, and PEDOT:PSS–rGO coated cotton fabrics was measured according to ASTM standard D-5034-11 strip test method (2017).[91] All the fabric samples were cut into strips according to the strip test method with specimen size according to standard specifications (5 × 2.5 cm) of the standard. The average values were calculated for the measurements of stress

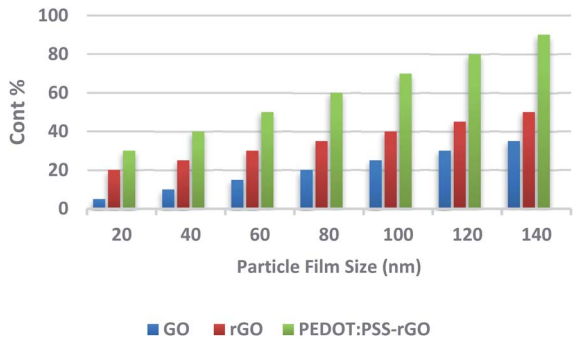

Fig. 3 Weight pick up% and particle size distribution of GO, rGO and PEDOT:PSS-rGO nano composite.

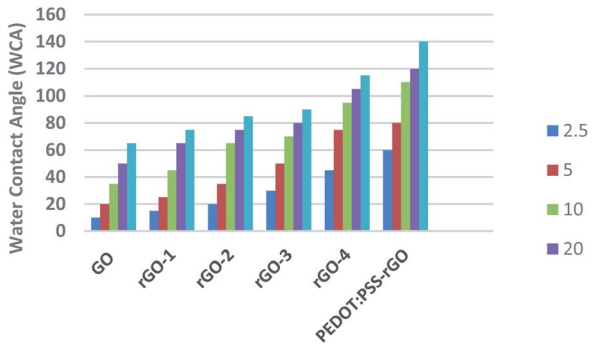

Fig. 4 Effect of different weight percent of GO, rGO and PEDOT:PSS-rGO nano composite on water contact angle.

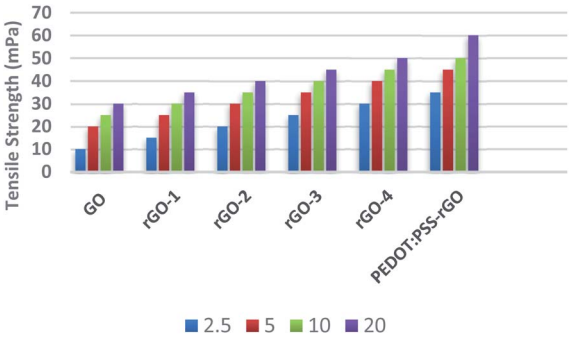

Fig. 5 Effect of different weight percent of GO, rGO and PEDOT:PSS on tensile strength of the coated fabric.

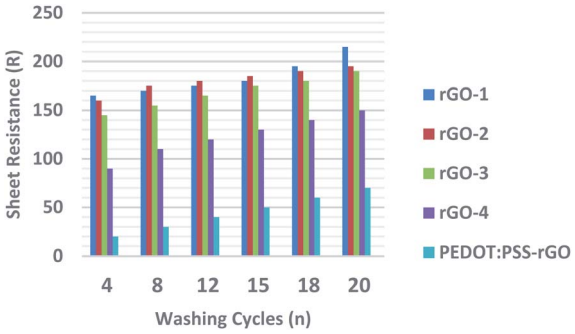

Fig. 7 Effect of washing cycles on electrical sheet resistance of as coated textile substrate with different weight percent of rGO and PEDOT:PSS-rGO nano composite.

(mPa) and strain (change in length) for both warp and weft directions of the fabrics. The resultant rGO coated fabric showed an increase in its strength of 10.0–20.0%, for initial 5 dyeing cycles and increased from 30.0–40.0% for 10 dyeing cycles, and 40.0–60.0% improvement for 10 padding cycles as shown in Fig. 5.

4.4 Sheet resistance

Electrical conductivity was measured according to ASTM standard 6343-2018 (ref. 92) in terms of sheet resistance of the as coated rGO, PEDOT:PSS–rGO nanocomposites. The electrical conductivity was measured using the following formula. $\sigma = 1/R \times t \times 0.34$; where "$\sigma$" is electrical conductivity, "R" is resistance, "t" is thickness and 0.34 is constant. The sheet resistance and electrical conductivity were performed using 2-probe, Keithley-2400 current source meter under ambient (20 °C) temperature and relative humidity (RH) of 65% ± 2. The results indicate that the change in sheet resistance was decreased as the padding cycle of rGO was increased as shown in the Fig. 6 and ESI-S2† which may attribute to the loading more rGO on the fabric, with higher interaction to provide the conduction channels on the textile substrate. Fig. 6 shows that the electrical performance was improved, when the number of dyeing cycles was increased to 20. The sheet resistance was decreased from 250–45 kΩ, which is attributable to the number of rGO nanosheets/films on the surface of fibres and cover the more free space which results in higher interaction between fibers as conductive paths.[93]

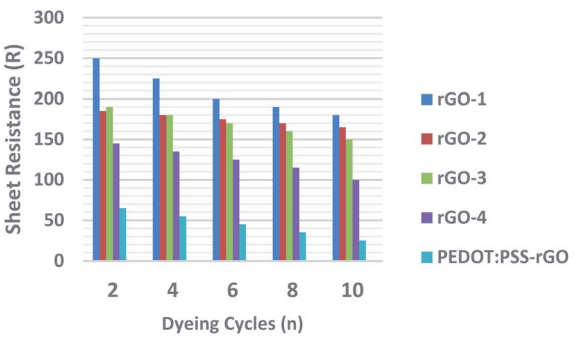

Fig. 6 Effect of different weight percent of GO, rGO and PEDOT:PSS on electrical sheet resistance of as coated fabric.

Whereas, the sheet resistance was found to be increased with number of 50 washing cycles, which is due to the removal of rGO sheets from the textile as shown in Fig. 7. The resultant PEDOT:PSS/rGO cotton fabric showed exceptional sheet resistance 15–45 (kΩ sq^{-1}) as show in (Table 3 ESI-S2†). The results indicate that the electrical performance was significantly influenced when the washing cycles were increased up to 20–50, this synergistic effect may occur due to the removal of rGO films from the free spaces in the fabric structure and fibers assembly in the yarn.

The PEDOT:PSS/rGO nano-hybrids coated fabric showed washing stability against several washes. Initially the sheet resistance was recorded as 185 kΩ sq^{-1}, which potentially decreased to 185 kΩ sq^{-1} with number of dyeing cycles of rGO as shown in Fig. 6 which may attribute to the higher binding and inter-bond facial interaction of rGO sheets with fiber surface. Finally, the sheet resistance of the rGO coated fabric was found further decreased to 185–125 kΩ sq^{-1} with the different weight percent of rGO with number of padding cycles. Table 2 clearly describes the effect of change in temperature and different wt%, which shows that, by increasing the content wt% of rGO significantly reduced the sheet resistance as result improved the electrical conductivity of the textile substrate.[94]

The results shown in Table 2 describe that, the content percent of rGO as a filler was increased, the electrical performance of the nanocomposites was also significantly improved. The sheet resistance dominantly decreased from 185–125 kΩ sq^{-1} to 115–40 kΩ sq^{-1} for different loading of rGO in PEDOT:PSS as compared to pristine rGO coated cotton fabric. The effect may be attributed to the higher inter facial bonding of polymer molecules with rGO nanosheets as well on the fiber surface. The sheet resistance was reduced to (125 kΩ) with 20% of rGO in PEDOT:PSS nanocomposites. See ESI-S2 Tables 5 and 6 respectively.†

4.5 Thermoelectric performance

The thermoelectric properties including an output power factor and Seebeck coefficient were calculated using the following formula, $F = S^2\sigma$; where, (S) is the Seebeck coefficient and sigma (σ) is electrical conductivity. The thermal gradient calculated using formula; $\Delta T = T_h - T_c/T_h$; whereas, (ΔT) is change in

Table 2 Reduced graphene oxide nanocomposites with different wt% of rGO

rGO (wt%)	rGO (kΩ sq^{-1})	PEDOT:PSS (kΩ sq^{-1})	PEDOT:PSS–rGO (Ω Sq^{-1})	Seebeck (μV K^{-1})	Power factor (μW m^{-1} K^{-2})
2.5	185	115 ± 5	85 ± 5	12.5	25
5.0	175	95 ± 5	75 ± 5	25.5	78
10.0	145	85 ± 5	45 ± 5	50.5	125
20.0	125	65 ± 5	25 ± 5	60.5	150

temperature between human body temperature as hot side (T_h) (36.5 °C) 309 K, and outside as cold side temperature is (T_c) (20 °C)/293–309 K. The Seebeck coefficient (S) was calculated with a change in voltage using the following formula, $S = \left(-\frac{\Delta V}{\Delta T}\right)$ whereas, S is Seebeck coefficient, ΔV is change in electric potential, ΔT is change in temperature or thermal gradient between hot and cold sides of TE device. All, the tests were performed in standard testing conditions with RH of 65 ± 2% and conditioned room temperature of 20 ± 2 °C. The performance measurements including thermal conductivity, Seebeck coefficient are provided in ESI-S3.†

4.5.1 Seebeck coefficient. The change in current was observed with the different content percent of rGO in PEDOT:PSS, the Seebeck coefficient was increased from 2.5–60.0 μV K^{-1} with a temperature difference of 16.5 °C over different dyeing cycle of rGO coated fabric as shown in Fig. 8. The Seebeck coefficient was increased with the change in temperature, which is attributed to a reduction in electrical conductivity and reduced thermal conductivity[95,96] as shown Fig. 8 and ESI-S2.†[95] The thermal conductivity, Seebeck coefficient and power factor of the resultant samples was increased due to the increase of rGO content percent in the PEDOT:PSS polymer as a filler.

The results show that, the thermoelectric performance including the Seebeck coefficient an power factor value were significantly increased with an increase in the change in temperature from 20 °C to 36.5 °C as a cold side with ambient testing conditions and human body temperature as hot side. The Seebeck coefficient (S_c) was increased from 12.5–60 μV K^{-1}, for the nano-hybrids over a temperature range of 290–309 K as shown in Fig. 8; which may be attributed content percent of rGO in conjugated conductive polymers as a filler and change in temperature as work function[98]. The results demonstrate that, the thermoelectric performance in terms of Seebeck coefficient and power factor is several order of magnitude higher when compare with previously reported textile based wearable TE devices.[99]

4.5.2 Power factor (PF). The results show that, when as fabricated e-textile TE model was directly placed onto human wrist without any masking. The developed TE device is capable to generate an open circuit output voltage of (0.5–12.5) mV and 9.5–19.5 (mV) for parallel and series arrangement with 6–8 TE legs connected with adhesive copper tape and conductive sewing thread respectively. The thermal gradient of 16.5 °C and output voltage of the as fabricated TE device was analysed under the ambient temperature (T_c) (20.0 ± 2 °C) as cold-side open to the air and (T_h) hot-side with a body temperature of (36.5 °C) next to the skin.[97] The TE nanogenerator, produced 2.5–9.5 mV per leg at room temperature, further increased to (19.5 mV per leg) with the change in temperature of 5 °C/298 K raised (2.5–9.5 mV K^{-1}) and maximum millivolt produced (75–120 mV) as shown in Fig. 9 and ESI-S2;† for series and parallel arrangement of the TEG legs.

4.5.3 Electric potential (mV). The resultant TEG nanogenerator showed exceptional performance to covert the thermal gradient of 16.5 °C between the human body heat (T_1 = 36.5 °C) and external temperature (T_2 = 20 °C) as an ambient testing condition, which is equals to the 293–309 K. The 2-leg TE nanogenerator is capable of produce the 2.5–9.5 mV at an ambient temperature 20 °C (293 K) temperature as cold side

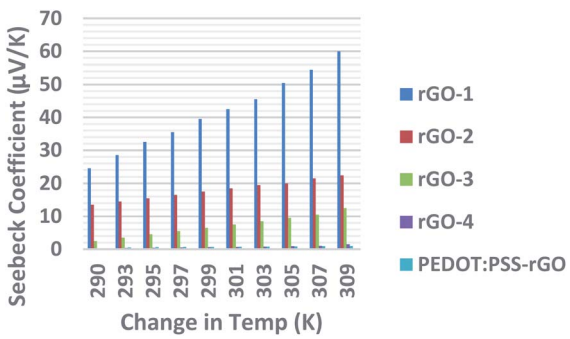

Fig. 8 Effect of temperature gradient on thermoelectric performance of as coated substrate with different weight percent of rGO and PEDOT:PSS nano composite.

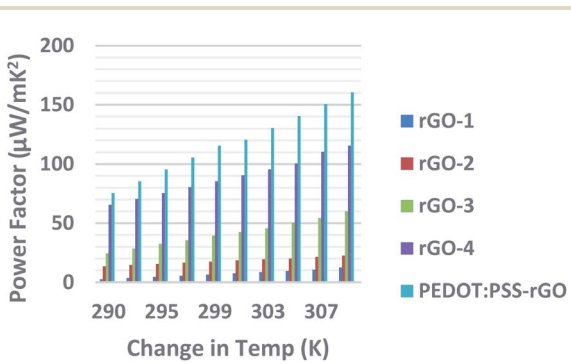

Fig. 9 Effect of temperature and different weight percent of rGO on thermoelectric performance power factor of textile substrate.

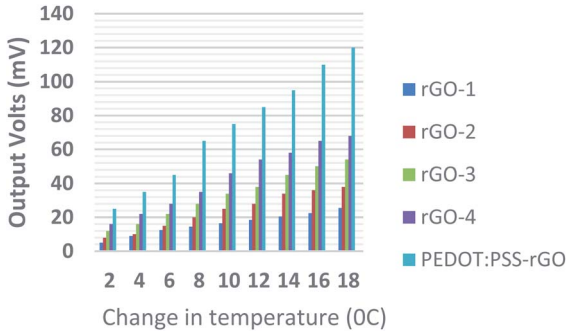

Fig. 10 Effect of temperature gradient on output electric potential (mV) as coated textile based TE device with different weight percent of rGO and PEDOT:PSS-rGO nano composite.

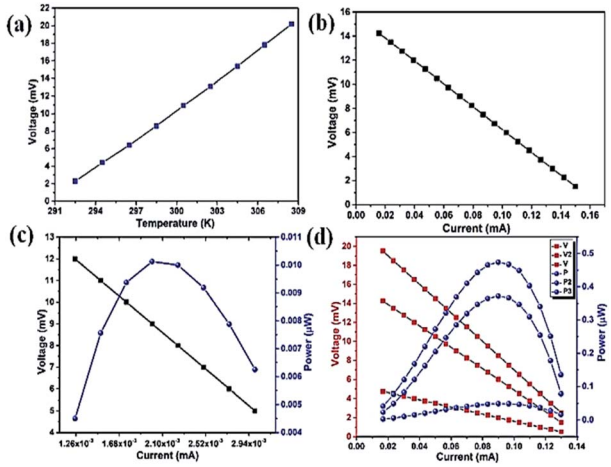

Fig. 11 Overall thermoelectric TE performance of textile based device, (a) output electric potential (mV) (b) current (mA) (c) voltage *vs.* current and power density (d) output electric potential and power of TE device with variable TE legs.

with a temperature difference (ΔT) of 16.5 °C between human body temperature as a hot side.[99] The p-type and n-type legs showed significant improvement in electric potential, with the change in millivolt from 19.5–120.0 mV when TE legs were increased from 6–8 legs as shown in Fig. 10.

The Fig. 10 shows the capability of the textile-based TEG nanogenerator to produce the electric potential (ΔV) with different weight percent of rGO and change in temperature (ΔT) of 1.0–16.5 ± 2 °C. The results indicate that the TE nanogenerator is capable of producing electric potential of 2.5–12.5 mV; when directly placed on the human wrist. The 2–4 TE legs were connected in parallel and series arrangements, the output electric potential was increased from (2.5–19.5) mV. An output power generated by the resultant TE generator was obtained as 2.5–9.5 mV 2-leg and 4-leg TE device over a thermal gradient of 293–300 K and capable to generate 12.5–120.0 mV, 293–309 K as shown in ESI-S2.† The current *versus* voltage relationship shows linear relationship compared to voltage and temperature relationship. The minimum circuit as an electric potential of 2.5–9.5 mV was obtained for each TE leg with a change in temperature gradient of 16.5 °C at ambient temperature of 20 °C, and the human body temperature. The 8–10 leg TE device produced 2.5–12.5 mV with a Seebeck coefficient of 2.5–60 ($\mu V\ K^{-1}$) developed in series and 8-leg device with power generation capacity of (25–160 $\mu W\ m^{-1}\ K^{-1}$), and current density of 0.05–0.15 (mA) over a thermal difference (ΔT) of 16.5 °C shown in ESI-S2.†

The TE device connected in a parallel arrangement using adhesive copper tape and conductive sewing thread for wearable device. The overall open circuit electrical potential (mV) was increased to 4.5–12.5 mV, with a power density of 0.0–0.5 ($\mu W\ K^{-1}$) as shown in Fig. 8c for a 2-leg TE device when attached to human body. The thermoelectric performance of TE device was improved and capable to produce the electric current of 0.02–0.14 (mA) with power factor of 0.0–0.5 (μW) as shown in Fig. 8d from the human body heat. The study demonstrates that the developed textile-based thermoelectric device can be used for health monitoring devices as self-powered e-textiles. The overall performance of TE generator device was further increased as the number of legs were increased 8–10. The overall maximum output voltage of (19.5–120) mV was obtained with 8–10 TE legs, when placed to human wrist and attached to digital voltmeter. The results clearly demonstrates the (*I*–*V*) relationship for open-circuit voltage induced by the thermoelectric effect of the fabricated device when placed to human body as shown in Fig. 11 and ESI-S2.†[100] The overall open circuit electrical potential (mV) was increased to 4.5–12.5 mV, with a power density of 25–160 ($\mu W\ m^{-1}\ K^{-1}$) as shown in Fig. 10 for a 2-leg TE device when attached to human body. The thermoelectric performance of TE device was improved and capable to produce the electric current of 0.02–0.15 (mA) shown in Fig. 9. The study demonstrates that the developed textile-based thermoelectric device can be used for health monitoring devices as self-powered e-textiles.

5. Conclusions

The fabrication of rGO coated cotton fabric was successfully developed using the industrial-scale pad–dry–cure method. The developed highly flexible and washable textile-based thermoelectric generator coated with PEDOT:PSS–rGO nanocomposites is highly efficient and suitable for energy harvesting from human body heat. The results demonstrate that the graphene and conductive polymer nanocomposite coated textile-based TE nanogenerator showed an improved TE performance with improved Seebeck coefficient (*S*), power factor with increasing the content percent of rGO in PEDOT:PSS–rGO nanocomposites. The results show that the Seebeck coefficients higher than 60 $\mu V\ K^{-1}$ was increased with increasing the number of dyeing cycles and the power factor was also significantly improved to 150 $\mu W\ m^{-1}\ K^{-2}$, with a temperature gradient of 16.5 °C (290–309 K) for PEDOT:PSS/rGO nanocomposite coated TE device. The output open circuit volts reached to 19.5–120 mV and 2.5–75 mV over a thermal difference between external and body temperature for series and parallel arrangements. This study demonstrates that fabrication of rGO and PEDOT:PSS/rGO nano-hybrids as thermoelectric

materials on textile substrate by using pad–dry–cure method is as an effective approach for the development of thermoelectric textiles.

Conflicts of interest

The authors declare no conflict of interest.

Acknowledgements

This work is acknowledged to Prof. Wang Jia Jun for his continuous guidelines and supervision. Author is also thankful China Scholarship Council during PhD studies at Zhejiang Sci-Tech University, Hangzhou, PR China.

References

1 Y. S. Chen and B. J. Lwo, Large-Area Laying of Soft Textile Power Generators for the Realization of Body Heat Harvesting Clothing, *Coatings*, 2019, **9**(12), 831.
2 N. D. Yilmaz, Introduction to Smart Nanotextiles, *Smart Textiles: Wearable Nanotechnology*, 2018, vol. 1.
3 J. S. Heo, J. Eom, Y. H. Kim and S. K. Park, Recent progress of textile-based wearable electronics: a comprehensive review of materials, devices, and applications, *Small*, 2018, **14**(3), 1703034.
4 A. Lund, Y. Tian, S. Darabi and C. Müller, A polymer-based textile thermoelectric generator for wearable energy harvesting, *J. Power Sources*, 2020, **480**, 228836.
5 Y. Lin, J. Liu, X. Wang, J. Xu, P. Liu, G. Nie and F. Jiang, An integral p-n connected all-graphene fiber boosting wearable thermoelectric energy harvesting, *Compos. Commun.*, 2019, **16**, 79–83.
6 L. Huang, S. Lin, Z. Xu, H. Zhou, J. Duan, B. Hu and J. Zhou, Fiber-based energy conversion devices for human-body energy harvesting, *Adv. Mater.*, 2020, **32**(5), 1902034.
7 X. Xu, J. Zhou and J. Chen, Thermal transport in conductive polymer-based materials, *Adv. Funct. Mater.*, 2020, **30**(8), 1904704.
8 Z. Lu, H. Zhang, C. Mao and C. M. Li, Silk fabric-based wearable thermoelectric generator for energy harvesting from the human body, *Appl. Energy*, 2016, **164**, 57–63.
9 Q. Wu and J. Hu, Waterborne polyurethane based thermoelectric composites and their application potential in wearable thermoelectric textiles, *Composites, Part B*, 2016, **107**, 59–66.
10 J. Liu, Y. Jia, Q. Jiang, F. Jiang, C. Li, X. Wang and J. Xu, Highly conductive hydrogel polymer fibers toward promising wearable thermoelectric energy harvesting, *ACS Appl. Mater. Interfaces*, 2018, **10**(50), 44033–44040.
11 V. Jangra, S. Maity and P. Vishnoi, A review on the development of conjugated polymer-based textile thermoelectric generator, *J. Ind. Text.*, 2021, 1528083721996732.
12 C. Zhang, Q. Zhang, D. Zhang, M. Wang, Y. Bo, X. Fan and Y. Chen, Highly Stretchable Carbon Nanotubes/Polymer Thermoelectric Fibers, *Nano Lett.*, 2021, **21**(2), 1047–1055.
13 M. Zhang, T. Gao, J. Wang, J. Liao, Y. Qiu, Q. Yang and L. Chen, A hybrid fibers based wearable fabric piezoelectric nanogenerator for energy harvesting application, *Nano Energy*, 2015, **13**, 298–305.
14 Y. Zhang and S. J. Park, Flexible organic thermoelectric materials and devices for wearable green energy harvesting, *Polymers*, 2019, **11**(5), 909.
15 Y. Zheng, Q. Zhang, W. Jin, Y. Jing, X. Chen, X. Han and C. Di, Organic Thermoelectric Textiles for Harvesting Thermal Energy and Powering Electronics, 2019, arXiv preprint arXiv:1907.04883.
16 G. Prunet, F. Pawula, G. Fleury, E. Cloutet, A. J. Robinson, G. Hadziioannou and A. Pakdel, A Review on Conductive Polymers and Their Hybrids for Flexible and Wearable Thermoelectric Applications, *Mater. Today Phys.*, 2021, 100402.
17 R. Torah, J. Lawrie-Ashton, Y. Li, S. Arumugam, H. A. Sodano and S. Beeby, Energy-harvesting materials for smart fabrics and textiles, *MRS Bull.*, 2018, **43**(3), 214–219.
18 C. Xu, Y. Song, M. Han and H. Zhang, Portable and wearable self-powered systems based on emerging energy harvesting technology, *Microsyst. Nanoeng.*, 2021, **7**(1), 1–14.
19 X. Zheng, Q. Hu, X. Zhou, W. Nie, C. Li and N. Yuan, Graphene-based fibers for the energy devices application: a comprehensive review, *Mater. Des.*, 2021, 109476.
20 S. Shin, R. Kumar, J. W. Roh, D. S. Ko, H. S. Kim, S. I. Kim and R. Chen, High-performance screen-printed thermoelectric films on fabrics, *Sci. Rep.*, 2017, **7**(1), 1–9.
21 N. Chakhchaoui, R. Farhan, Y. M. Chu, U. Khan, A. Eddiai, L. E. H. Omari and Y. Boughaleb, Flexible smart textile coated by PVDF/graphene oxide with excellent energy harvesting toward a novel class of self-powered sensors: fabrication, characterization and measurements, 2021, DOI: 10.20944/preprints202103.0786.v3.
22 T. Jing, B. Xu and Y. Yang, Organogel electrode based continuous fiber with large-scale production for stretchable triboelectric nanogenerator textiles, *Nano Energy*, 2021, **84**, 105867.
23 H. T. Deng, X. R. Zhang, Z. Y. Wang, D. L. Wen, Y. Y. Ba, B. Kim and X. S. Zhang, Super-stretchable multi-sensing triboelectric nanogenerator based on liquid conductive composite, *Nano Energy*, 2021, **83**, 105823.
24 T. Busolo, P. K. Szewczyk, M. Nair, U. Stachewicz and S. Kar-Narayan, Triboelectric Yarns with Electrospun Functional Polymer Coatings for Highly Durable and Washable Smart Textile Applications, *ACS Appl. Mater. Interfaces*, 2021, **13**(14), 16876–16886.
25 L. Wang and K. Zhang, Textile-based thermoelectric generators and their applications, *Energy Environ. Mater.*, 2020, **3**(1), 67–79.
26 Y. Wang, L. Yang, X. L. Shi, X. Shi, L. Chen, M. S. Dargusch and Z. G. Chen, Flexible thermoelectric materials and generators: challenges and innovations, *Adv. Mater.*, 2019, **31**(29), 1807916.
27 W. Y. Chen, X. L. Shi, J. Zou and Z. G. Chen, Wearable fiber-based thermoelectrics from materials to applications, *Nano Energy*, 2020, 105684.

28 S. Lin, W. Li and Y. Pei, Thermally insulative thermoelectric argyrodites, *Mater. Today*, 2021, DOI: 10.1016/j.mattod.2021.01.007.
29 Y. Wang, S. Liu, Z. Wu, G. Liu, X. Yang, T. Wei and J. Zhu, Enhanced thermoelectric performance of van der Waals tellurium via vacancy engineering, *Mater. Today Phys.*, 2021, **18**, 100379.
30 C. Qin, M. Jin, R. Zhang, L. Zhou, X. Bai, M. Yang and W. Li, Preparation and thermoelectric properties of ZnTe-doped Bi0. 5Sb1. 5Te3 single crystal, *Mater. Lett.*, 2021, **292**, 129619.
31 L. K. Allison and T. L. Andrew, A wearable all-fabric thermoelectric generator, *Adv. Mater. Technol.*, 2019, **4**(5), 1800615.
32 T. Gao, Z. Yang, C. Chen, Y. Li, K. Fu, J. Dai and L. Hu, Three-dimensional printed thermal regulation textiles, *ACS Nano*, 2017, **11**(11), 11513–11520.
33 S. J. Kim, J. H. We and B. J. Cho, A wearable thermoelectric generator fabricated on a glass fabric, *Energy Environ. Sci.*, 2014, **7**(6), 1959–1965.
34 J. Shi, S. Liu, L. Zhang, B. Yang, L. Shu, Y. Yang and X. Tao, Smart textile-integrated microelectronic systems for wearable applications, *Adv. Mater.*, 2020, **32**(5), 1901958.
35 L. Wang, Z. Zhang, L. Geng, T. Yuan, Y. Liu, J. Guo and S. Wang, Solution-printable fullerene/TiS_2 organic/inorganic hybrids for high-performance flexible n-type thermoelectrics, *Energy Environ. Sci.*, 2018, **11**(5), 1307–1317.
36 J. D. Ryan, A. Lund, A. I. Hofmann, R. Kroon, R. Sarabia-Riquelme, M. C. Weisenberger and C. Müller, All-organic textile thermoelectrics with carbon-nanotube-coated n-type yarns, *ACS Appl. Energy Mater.*, 2018, **1**(6), 2934–2941.
37 H. Xu, Y. Guo, B. Wu, C. Hou, Q. Zhang, Y. Li and H. Wang, Highly Integrable Thermoelectric Fiber, *ACS Appl. Mater. Interfaces*, 2020, **12**(29), 33297–33304.
38 Y. Yang, G. Zhao, X. Cheng, H. Deng and Q. Fu, Stretchable and Healable Conductive Elastomer Based on PEDOT:PSS/Natural Rubber for Self-Powered Temperature and Strain Sensing, *ACS Appl. Mater. Interfaces*, 2021, **13**(12), 14599–14611.
39 T. Sun, B. Zhou, Q. Zheng, L. Wang, W. Jiang and G. J. Snyder, Stretchable fabric generates electric power from woven thermoelectric fibers, *Nat. Commun.*, 2020, **11**(1), 1–10.
40 T. Juntunen, H. Jussila, M. Ruoho, S. Liu, G. Hu, T. Albrow-Owen and I. Tittonen, Inkjet printed large-area flexible few-layer graphene thermoelectrics, *Adv. Funct. Mater.*, 2018, **28**(22), 1800480.
41 N. Nandihalli, C. J. Liu and T. Mori, Polymer based thermoelectric nanocomposite materials and devices: fabrication and characteristics, *Nano Energy*, 2020, 105186.
42 T. G. Novak, K. Kim and S. Jeon, 2D and 3D nanostructuring strategies for thermoelectric materials, *Nanoscale*, 2019, **11**(42), 19684–19699.
43 D. Ding, F. Sun, F. Xia and Z. Tang, A high-performance and flexible thermoelectric generator based on the solution-processed composites of reduced graphene oxide nanosheets and bismuth telluride nanoplates, *Nanoscale Adv.*, 2020, **2**(8), 3244–3251.
44 A. Ahmed, M. A. Jalil, M. M. Hossain, M. Moniruzzaman, B. Adak, M. T. Islam and S. Mukhopadhyay, A PEDOT:PSS and graphene-clad smart textile-based wearable electronic Joule heater with high thermal stability, *J. Mater. Chem. C*, 2020, **8**(45), 16204–16215.
45 B. Lee, H. Cho, K. T. Park, J. S. Kim, M. Park, H. Kim and S. Chung, High-performance compliant thermoelectric generators with magnetically self-assembled soft heat conductors for self-powered wearable electronics, *Nat. Commun.*, 2020, **11**(1), 1–12.
46 M. G. Tadesse, D. A. Mengistie, Y. Chen, L. Wang, C. Loghin and V. Nierstrasz, Electrically conductive highly elastic polyamide/lycra fabric treated with PEDOT:PSS and polyurethane, *J. Mater. Sci.*, 2019, **54**(13), 9591–9602.
47 J. Choi, Y. Jung, S. J. Yang, J. Y. Oh, J. Oh, K. Jo and H. Kim, Flexible and robust thermoelectric generators based on all-carbon nanotube yarn without metal electrodes, *ACS Nano*, 2017, **11**(8), 7608–7614.
48 T. Zhang, K. Li, J. Zhang, M. Chen, Z. Wang, S. Ma and L. Wei, High-performance, flexible, and ultralong crystalline thermoelectric fibers, *Nano Energy*, 2017, **41**, 35–42.
49 A. Yadav, K. P. Pipe and M. Shtein, Fiber-based flexible thermoelectric power generator, *J. Power Sources*, 2008, **175**(2), 909–913.
50 L. K. Allison and T. L. Andrew, A wearable all-fabric thermoelectric generator, *Adv. Mater. Technol.*, 2019, **4**(5), 1800615.
51 T. Zhang, K. Li, J. Zhang, M. Chen, Z. Wang, S. Ma and L. Wei, High-performance, flexible, and ultralong crystalline thermoelectric fibers, *Nano Energy*, 2017, **41**, 35–42.
52 C. J. An, Y. H. Kang, H. Song, Y. Jeong and S. Y. Cho, High-performance flexible thermoelectric generator by control of electronic structure of directly spun carbon nanotube webs with various molecular dopants, *J. Mater. Chem. A*, 2017, **5**(30), 15631–15639.
53 C. J. An, Y. C. Lee, Y. H. Kang and S. Y. Cho, Improved interaction between semiconducting polymer and carbon nanotubes in thermoelectric composites through covalent grafting, *Carbon*, 2017, **124**, 662–668.
54 C. J. An, Y. H. Kang, A. Y. Lee, K. S. Jang, Y. Jeong and S. Y. Cho, Foldable thermoelectric materials: improvement of the thermoelectric performance of directly spun CNT webs by individual control of electrical and thermal conductivity, *ACS Appl. Mater. Interfaces*, 2016, **8**(34), 22142–22150.
55 G. Wu, C. Gao, G. Chen, X. Wang and H. Wang, High-performance organic thermoelectric modules based on flexible films of a novel n-type single-walled carbon nanotube, *J. Mater. Chem. A*, 2016, **4**(37), 14187–14193.
56 Y. H. Kang, U. H. Lee, I. H. Jung, S. C. Yoon and S. Y. Cho, Enhanced thermoelectric performance of conjugated polymer/CNT nanocomposites by modulating the

potential barrier difference between conjugated polymer and CNT, *ACS Appl. Electron. Mater.*, 2019, **1**(7), 1282–1289.

57 L. Wang, Z. Zhang, L. Geng, T. Yuan, Y. Liu, J. Guo and S. Wang, Solution-printable fullerene/TiS_2 organic/inorganic hybrids for high-performance flexible n-type thermoelectrics, *Energy Environ. Sci.*, 2018, **11**(5), 1307–1317.

58 Y. Du, K. Cai, S. Chen, H. Wang, S. Z. Shen, R. Donelson and T. Lin, Thermoelectric fabrics: toward power generating clothing, *Sci. Rep.*, 2015, **5**(1), 1–6.

59 A. Ahmed, M. A. Jalil, M. M. Hossain, M. Moniruzzaman, B. Adak, M. T. Islam and S. Mukhopadhyay, A PEDOT:PSS and graphene-clad smart textile-based wearable electronic Joule heater with high thermal stability, *J. Mater. Chem. C*, 2020, **8**(45), 16204–16215.

60 C. Yeon, G. Kim, J. W. Lim and S. J. Yun, Highly conductive PEDOT:PSS treated by sodium dodecyl sulfate for stretchable fabric heaters, *RSC Adv.*, 2017, **7**(10), 5888–5897.

61 X. He, R. He, Q. Lan, W. Wu, F. Duan, J. Xiao and J. Liu, Screen-printed fabrication of PEDOT:PSS/silver nanowire composite films for transparent heaters, *Materials*, 2017, **10**(3), 220.

62 H. M. Elmoughni, A. K. Menon, R. M. Wolfe and S. K. Yee, A textile-integrated polymer thermoelectric generator for body heat harvesting, *Adv. Mater. Technol.*, 2019, **4**(7), 1800708.

63 J. Liu, G. Liu, J. Xu, C. Liu, W. Zhou, P. Liu and F. Jiang, Graphene/Polymer Hybrid Fiber with Enhanced Fracture Elongation for Thermoelectric Energy Harvesting, *ACS Appl. Energy Mater.*, 2020, **3**(7), 6165–6171.

64 X. Pu, L. Li, M. Liu, C. Jiang, C. Du, Z. Zhao and Z. L. Wang, Wearable self-charging power textile based on flexible yarn supercapacitors and fabric nanogenerators, *Adv. Mater.*, 2016, **28**(1), 98–105.

65 K. Jost, D. Stenger, C. R. Perez, J. K. McDonough, K. Lian, Y. Gogotsi and G. Dion, Knitted and screen printed carbon-fiber supercapacitors for applications in wearable electronics, *Energy Environ. Sci.*, 2013, **6**(9), 2698–2705.

66 X. Zheng, J. Shen, Q. Hu, W. Nie, Z. Wang, L. Zou and C. Li, Vapor phase polymerized conducting polymer/MXene textiles for wearable electronics, *Nanoscale*, 2021, **13**(3), 1832–1841.

67 A. Dey, O. P. Bajpai, A. K. Sikder, S. Chattopadhyay and M. A. S. Khan, Recent advances in CNT/graphene based thermoelectric polymer nanocomposite: a proficient move towards waste energy harvesting, *Renewable Sustainable Energy Rev.*, 2016, **53**, 653–671.

68 J. A. Lee, A. E. Aliev, J. S. Bykova, M. J. de Andrade, D. Kim, H. J. Sim and R. H. Baughman, Woven-yarn thermoelectric textiles, *Adv. Mater.*, 2016, **28**(25), 5038–5044.

69 Y. Zheng, Q. Zhang, W. Jin, Y. Jing, X. Chen, X. Han and C. Di, Organic Thermoelectric Textiles for Harvesting Thermal Energy and Powering Electronics, 2019, arXiv preprint arXiv:1907.04883.

70 F. Deng, H. Qiu, J. Chen, L. Wang and B. Wang, Wearable thermoelectric power generators combined with flexible supercapacitor for low-power human diagnosis devices, *IEEE Trans. Ind. Electron.*, 2016, **64**(2), 1477–1485.

71 R. Torah, J. Lawrie-Ashton, Y. Li, S. Arumugam, H. A. Sodano and S. Beeby, Energy-harvesting materials for smart fabrics and textiles, *MRS Bull.*, 2018, **43**(3), 214–219.

72 M. B. Kale, Z. Luo, X. Zhang, D. Dhamodharan, N. Divakaran, S. Mubarak and Y. Xu, Waterborne polyurethane/graphene oxide-silica nanocomposites with improved mechanical and thermal properties for leather coatings using screen printing, *Polymer*, 2019, **170**, 43–53.

73 G. B. Tseghai, D. A. Mengistie, B. Malengier, K. A. Fante and L. Van Langenhove, PEDOT:PSS-based conductive textiles and their applications, *Sensors*, 2020, **20**(7), 1881.

74 N. Bisht, P. More, P. K. Khanna, R. Abolhassani, Y. K. Mishra and M. Madsen, Progress of hybrid nanocomposite materials for thermoelectric applications, *Mater. Adv.*, 2021, **2**, 1927–1956.

75 Y. J. Yun, H. J. Lee, T. H. Son, H. Son and Y. Jun, Mercerization to enhance flexibility and electromechanical stability of reduced graphene oxide cotton yarns, *Compos. Sci. Technol.*, 2019, **184**, 107845.

76 D. P. Dubal, N. R. Chodankar, D. H. Kim and P. Gomez-Romero, Towards flexible solid-state supercapacitors for smart and wearable electronics, *Chem. Soc. Rev.*, 2018, **47**(6), 2065–2129.

77 R. Islam, N. Khair, D. M. Ahmed and H. Shahariar, Fabrication of low cost and scalable carbon-based conductive ink for E-textile applications, *Mater. Today Commun.*, 2019, **19**, 32–38.

78 X. Wang, A. K. K. Kyaw, C. Yin, F. Wang, Q. Zhu, T. Tang and J. Xu, Enhancement of thermoelectric performance of PEDOT:PSS films by post-treatment with a superacid, *RSC Adv.*, 2018, **8**(33), 18334–18340.

79 N. Nandihalli, C. J. Liu and T. Mori, Polymer based thermoelectric nanocomposite materials and devices: fabrication and characteristics, *Nano Energy*, 2020, 105186.

80 C. Dagdeviren, Z. Li and Z. L. Wang, Energy harvesting from the animal/human body for self-powered electronics, *Annu. Rev. Biomed. Eng.*, 2017, **19**, 85–108.

81 S. Lee, S. Kim, A. Pathak, A. Tripathi, T. Qiao, Y. Lee and H. Y. Woo, Recent progress in organic thermoelectric materials and devices, *Macromol. Res.*, 2020, **28**(6), 531–552.

82 I. Petsagkourakis, K. Tybrandt, X. Crispin, I. Ohkubo, N. Satoh and T. Mori, Thermoelectric materials and applications for energy harvesting power generation, *Sci. Technol. Adv. Mater.*, 2018, **19**(1), 836–862.

83 N. Van Toan, T. T. K. Tuoi and T. Ono, Thermoelectric generators for heat harvesting: from material synthesis to device fabrication, *Energy Convers. Manage.*, 2020, **225**, 113442.

84 J. H. Kim and T. J. Kang, Composite films of poly(3,4-ethylenedioxythiophene) polystyrene sulfonate incorporated with carbon nanotube sheet for improved power factor in thermoelectric conversion, *Mater. Today Commun.*, 2020, **25**, 101568.

85 Y. Du, K. F. Cai, S. Chen, P. Cizek and T. Lin, Facile preparation and thermoelectric properties of Bi_2Te_3 based alloy nanosheet/PEDOT:PSS composite films, *ACS Appl. Mater. Interfaces*, 2014, **6**(8), 5735–5743.

86 Y. S. Chen and B. J. Lwo, Large-Area Laying of Soft Textile Power Generators for the Realization of Body Heat Harvesting Clothing, *Coatings*, 2019, **9**(12), 831.

87 J. Yan, S. Li, B. Lan, Y. Wu and P. S. Lee, Rational Design of Nanostructured Electrode Materials toward Multifunctional Supercapacitors, *Adv. Funct. Mater.*, 2019, 1902564.

88 Z. Stempien, M. Khalid, M. Kozicki, M. Kozanecki, H. Varela, P. Filipczak and E. Sąsiadek, In situ deposition of reduced graphene oxide layers on textile surfaces by the reactive inkjet printing technique and their use in supercapacitor applications, *Synth. Met.*, 2019, **256**, 116144.

89 E. T. Alonso, D. P. Rodrigues, M. Khetani, D. W. Shin, A. De Sanctis, H. Joulie and S. Russo, Graphene electronic fibres with touch-sensing and light-emitting functionalities for smart textiles, *npj Flexible Electron.*, 2018, **2**(1), 1–6.

90 K. Dong, Y. C. Wang, J. Deng, Y. Dai, S. L. Zhang, H. Zou and Z. L. Wang, A highly stretchable and washable all-yarn-based self-charging knitting power textile composed of fiber triboelectric nanogenerators and supercapacitors, *ACS Nano*, 2017, **11**(9), 9490–9499.

91 S. B. Jeon, S. J. Park, W. G. Kim, I. W. Tcho, I. K. Jin, J. K. Han and Y. K. Choi, Self-powered wearable keyboard with fabric based triboelectric nanogenerator, *Nano energy*, 2018, **53**, 596–603.

92 Z. Cui, Silver Nanowire-based Flexible and Stretchable Devices: Applications and Manufacturing, Doctor of Philosophy, North Carolina State University, 2019.

93 N. He, *Graphene-Based Functional Fibers and Their Applications in Energy-Storage Textiles*, 2018.

94 X. Pu, W. Hu and Z. L. Wang, Toward wearable self-charging power systems: the integration of energy-harvesting and storage devices, *Small*, 2018, **14**(1), 1702817.

95 S. Bhattacharjee, R. Joshi, A. A. Chughtai and C. R. Macintyre, Graphene Modified Multifunctional Personal Protective Clothing, *Adv. Mater. Interfaces*, 2019, **6**(21), 1900622.

96 Y. Yin, Y. Xu and C. Wang, Functionalization of Fiber Materials for Washable Smart Wearable Textiles, *Flexible and Wearable Electronics for Smart Clothing*, 2020, pp. 183–212.

97 F. Tehrani, M. Beltrán-Gastélum, K. Sheth, A. Karajic, L. Yin, R. Kumar and M. Mueller, Laser-Induced Graphene Composites for Printed, Stretchable, and Wearable Electronics, *Adv. Mater. Technol.*, 2019, **4**(8), 1900162.

98 B. Baruah and A. Kumar, Electrocatalytic Activity of rGO/PEDOT:PSS Nanocomposite towards Methanol Oxidation in Alkaline Media, *Electroanalysis*, 2018, **30**(9), 2131–2144.

99 F. Brunetti, A. Operamolla, S. Castro-Hermosa, G. Lucarelli, V. Manca, G. M. Farinola and T. M. Brown, Printed solar cells and energy storage devices on paper substrates, *Adv. Funct. Mater.*, 2019, **29**(21), 1806798.

100 J. Shi, S. Liu, L. Zhang, B. Yang, L. Shu, Y. Yang and Y. Chai, Smart Textile-Integrated Microelectronic Systems for Wearable Applications, *Adv. Mater.*, 2019, 1901958.